Volume 16 | Number 45 | 7 December 2014 | Pages 24637–25202

PCCP

Physical Chemistry Chemical Physics

www.rsc.org/pccp

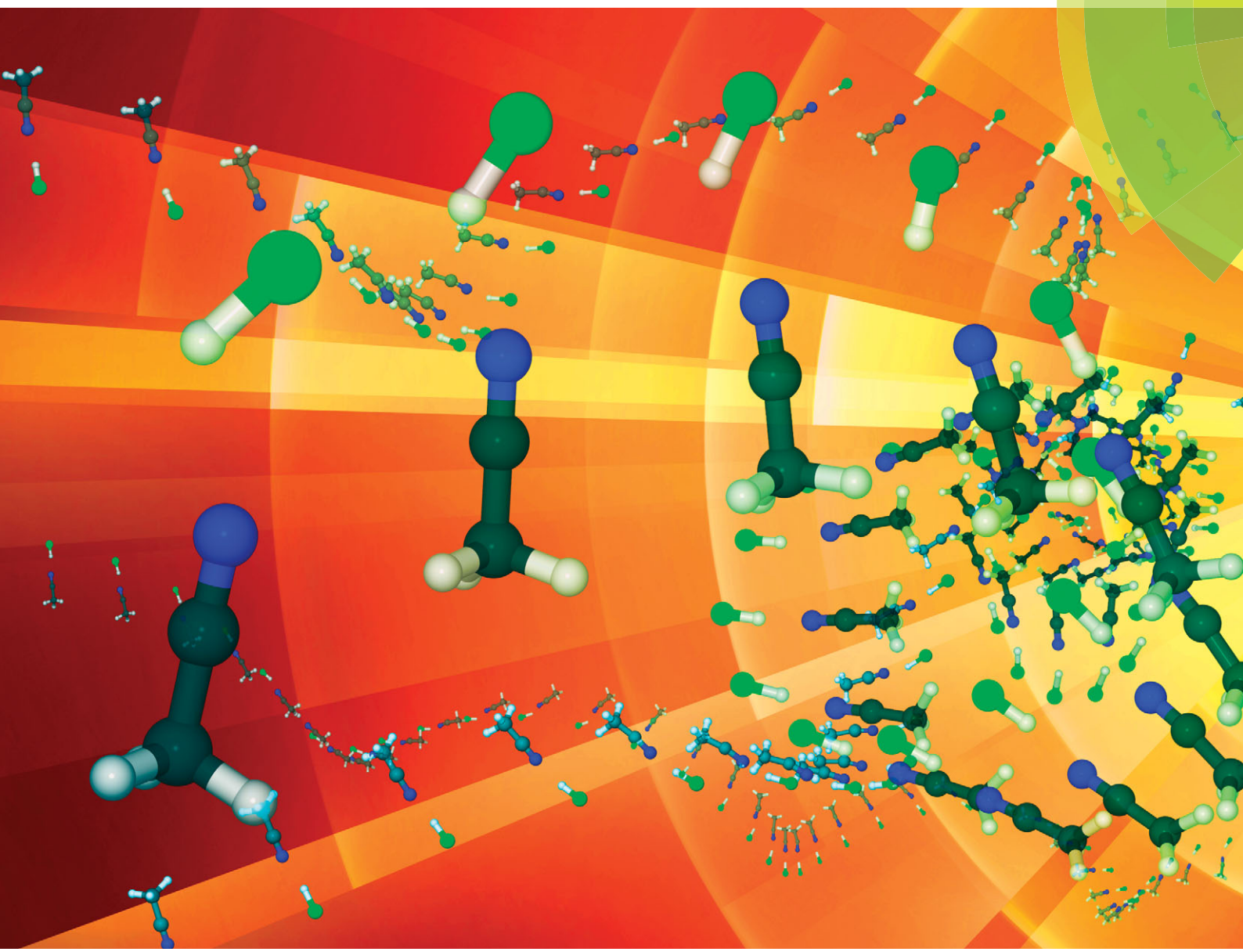

ISSN 1463-9076

ROYAL SOCIETY OF CHEMISTRY

PAPER

Nicolai Bork *et al.*

Resolving the anomalous infrared spectrum of the MeCN–HCl molecular cluster using ab *Initio* molecular dynamics

PCCP

PAPER

View Article Online
View Journal | View Issue

Cite this: *Phys. Chem. Chem. Phys.*, 2014, **16**, 24685

Resolving the anomalous infrared spectrum of the MeCN–HCl molecular cluster using *ab Initio* molecular dynamics†

Nicolai Bork,*[ab] Ville Loukonen,[a] Henrik G. Kjaergaard[b] and Hanna Vehkamäki[a]

Received 26th August 2014,
Accepted 3rd October 2014

DOI: 10.1039/c4cp03828b

www.rsc.org/pccp

We present a molecular dynamics (MD) based study of the acetonitrile–hydrogen chloride molecular cluster in the gas phase, aimed at resolving the anomalous features often seen in infrared spectra of hydrogen bonded complexes. We find that the infrared spectrum obtained from the Fourier transform of the electric dipole moment autocorrelation function converges very slowly due to the floppy nature of the complex. Even after 55 picoseconds of simulation, significant differences in the modelled and experimental spectrum are seen, likely due to insufficient configurational sampling. Instead, we utilize the MD trajectory for a structural based analysis. We find that the most populated values of the N–H–Cl angle are around 162°. The global minimum energy conformation at 180.0° is essentially unpopulated. We re-model the spectrum by combining population data from the MD simulations with optimizations constraining the N–H–Cl angle. This re-modelled spectrum is in excellent accordance with the experimental spectrum and we conclude that the observed spectral anomaly is due to the dynamics of the N–H–Cl angle.

1 Introduction

One of the most abundant forms of molecular interaction is hydrogen bonding, *i.e.* the bonding of a hydrogen donor (Lewis acid, A-H) to a hydrogen acceptor (Lewis base, B).[1] Hydrogen bond strengths vary from very weak bonds, such as in the water dimer,[2] to very strong bonds, such as acids bonding to bases.[3] The latter case has recently gained much attention in the field of aerosol science, since it has been realized that clustering of sulfuric acid with nitrogenous bases *via* hydrogen bonds can lead to very efficient aerosol particle formation.[4–6]

Infrared (IR) spectroscopy is one of the most important and useful experimental techniques for exploring properties of hydrogen bonded molecular complexes. Spectra of numerous complexes have been obtained and the origin of most spectral features are readily explained, including the redshifted peak of the A–H stretch mode in the A–H···B complex.[7–16]

It is well known that most vibrationally excited states are short lived, and that their energy levels therefore can not be determined exactly due to the uncertainty principle. This results in Lorentzian shaped spectral peaks which tend to hide the underlying rotational structure of most hydrogen bonded complexes. However, lineshapes of hydrogen bonded complexes often deviate from Lorentzian possibly due to deviation of the A–H stretch potential in the A–H···B complex from the typical diatomic anharmonic potential. Alternatively, the non-Lorentzian shape may be due to coupling of the fundamental A–H stretch mode to other modes, *e.g.* intermolecular A–B vibrations, for example seen in the water dimer.[17]

We have recently published IR spectra of the hydrogen bonded molecular complex between HCl and acetonitrile (MeCN).[16] This is one of the best model system representing atmospheric acid–base clustering studied by IR spectroscopy to date. In this system, we found a highly unusual spectral shape associated with the fundamental H–Cl stretch mode in the complex. Since the fundamental A–H stretch mode is the most important spectral feature for characterizing hydrogen bonded complexes it is of interest to investigate this particular system and its IR spectrum in detail and to solve the nature of the unusual spectral shape.

Ab initio electronic structure calculations, in particular density functional theory (DFT), is now a standard approach for interpreting IR spectra. The main approach is to predict vibrational frequencies and intensities using the harmonic oscillator approximation based on the global minimum energy structure at 0 K. For most simple systems this is adequate for assigning fundamental modes, but by construction, the standard approach is neither able to predict spectral shapes (beyond simple addition of intensities of closely spaced modes), nor is it able to determine intensities of combination modes and overtones. For this, more advanced methods such as

[a] *Department of Physics, University of Helsinki, FI-00014 Helsinki, Finland. E-mail: nicolai.bork@helsinki.fi; Tel: +358 50 318 2219*
[b] *Department of Chemistry, University of Copenhagen, Universitetsparken 5, DK-2100 Copenhagen O, Denmark*

† Electronic supplementary information (ESI) available. See DOI: 10.1039/c4cp03828b

vibrational perturbation theory,[18] molecular dynamics (MD) simulations,[19] or reduced dimensionality local mode simulations[20] have been used with success.

IR spectra of numerous gas phase and solvated molecules have been modelled using MD simulations. However, only few spectra of hydrogen bonded complexes in the gas phase have been modelled[21] and, to the best of our knowledge, no comparisons between MD based and experimental spectra of such systems have been made. It is therefore of interest to investigate the feasibility of using MD simulations for predicting and reproducing spectra of such systems in greater detail. This study is therefore dedicated to a detailed investigation of the spectral lineshape of the H–Cl stretch mode in the MeCN–HCl molecular complex using MD simulations.

2 Computational methods

Besides the initial nuclear positions and velocities, MD uses the forces acting on each atom at each point of the simulation. Forces must be calculated using either a pre-defined force field or using electronic structure calculations (most often DFT). The latter approach is inherently CPU expensive, but generally yields the most accurate forces and provides a direct method for investigating phenomena related to molecular motion.[22]

For modelling IR spectra, the electric dipole moment is the main molecular property of interest since the observable spectral absorption originate from dipole moment oscillations. The frequency dependent infrared absorbance, $A(\omega)$, can thus be calculated as the Fourier transform of the dipole moment autocorrelation function, $C(t)$, as

$$A(\omega) \propto \beta\hbar\omega(1 - \exp(-\beta\hbar\omega))D(\omega)\int C(t)\cos(\omega t)\mathrm{d}t \qquad (1)$$

where $\beta = (k_B T)^{-1}$, k_B is Boltzmann constant, T is temperature, $\hbar$ is the reduced Planck's constant, ω is the vibrational frequency (in s^{-1}), $D(\omega)$ is a quantum correction factor, and t is the time of the MD simulation (in seconds).[23] Since most spectroscopic data is reported in wavenumbers rather than in frequencies, we will use this unit *via* the conversion $\tilde{\nu} = \omega(2\pi c)^{-1}$ where c is the speed of light. The autocorrelation function is calculated as

$$C(t) = \langle \mu(t_0)\mu(t_0 + t)\rangle \qquad (2)$$

where μ is the total electric dipole moment. The angular brackets denotes the average of time origins t_0 and time separations t, restricted to $t \in \{0, t_{max}/2\}$ to ensure proper statistics for all t and $t_0 \leq t_{max} - t$, where t_{max} denote the length of the MD run.

The variability of the dipole moment giving rise to the IR spectrum originates from nuclear movement at identical periodicity. Hence, Fourier transformed atomic velocity autocorrelation functions are useful for interpreting the modelled spectrum, yielding the velocity density of states (VDOS). Similar to eqn (1), this is given as,

$$\mathrm{VDOS}_i(\omega) = \int \langle v_i(t_0)v_i(t_0 + t)\rangle \cos(\omega t)\mathrm{d}t \qquad (3)$$

where v_i denote the velocity of atom i.[19]

Related to this approach, we emphasize some basic points:

- Both fundamental modes, combination modes and overtones are obtainable from $A(\omega)$, but rotational structures are not.
- The magnitudes of signals in $A(\omega)$ and signals in VDOS(ω) are unrelated.
- A signal in VDOS(ω) does not necessitate a dipole moment change and hence a signal in $A(\omega)$.
- A signal in $A(\omega)$ necessitate a signal in VDOS(ω) since, no dipole moment change is possible without nuclear movement.

The MD simulations were conducted using the CP2K software package.[24,25] We used the Quickstep module of CP2K to calculate the electronic energies and the forces from DFT. Quickstep uses atom centred basis functions to represent the wavefunction, while the electronic density is represented by plane wave basis functions on regular grids.[26,27]

As in two related studies,[28,29] we chose to use the density functional by Perdew, Burke, and Ernzerhof (PBE).[30] The PBE functional has repeatedly been shown to be amongst the most stable DFT functionals for a range of properties, including structures and energies of gaseous clusters.[31,32] Dispersion forces are known to contribute significantly to hydrogen bonded systems, but are poorly described by DFT, so we used the D3 dispersion correctional scheme by Grimme *et al.*[33] In our previous study of the MeCN–HCl system,[16] the D3 correctional scheme was found to improve B3LYP calculations by *ca.* four kJ mol^{-1}, adding to the reliability of the D3 scheme although a different functional is being used in this study.

Periodic boundary conditions were not used and care was taken to prevent un-physical box boundary effects.[34] Testing showed that a box size of $(30\ \text{Å})^3$ was sufficiently large (Fig. S1, ESI†). Further testing showed that plane wave basis functions could be truncated at 450 Rydbergs and that augmented, triple-ζ, double polarized basis sets (aug-TZV2P)[25] could be used without the calculations becoming excessively CPU expensive (Fig. S2, ESI†).

To simulate most efficiently the experimental conditions, a temperature of 300 K was maintained using the Nosé–Hoover chain thermostat coupled to each Cartesian degree of freedom with a time constant of 11 fs.[35] The spectral region of interest is below *ca.* 3000 cm^{-1}, so requiring a resolution of at least 20 data points per vibration, a 0.5 fs time step was necessary. The simulation was continued for 120,000 MD steps (60 picoseconds), requiring *ca.* 85,000 CPU hours (*ca.* 5 seconds per step, parallelized on 516 processors).

We tested calculating the dipole moments using the standard operator implemented in CP2K *versus* using maximally localized Wannier function centres.[36] These methods were observed to perform similarly, and we chose to use the former method as the computational burden was smaller, enabling dipole moment evaluation in each step.

Several formulations of the quantum correction factor in eqn (1) has been proposed to account for detailed balance and spectral broadening including $D(\omega) = \beta\hbar\omega(1 - \exp(-\beta\hbar\omega))^{-1}$, $D(\omega) = \exp(0.5\beta\hbar\omega)$, $D(\omega) = 2(1 + \exp(-\beta\hbar\omega))^{-1}$ and $D(\omega) = \beta\hbar\omega(2\tanh(0.5\beta\hbar\omega))^{-1}$.[37] Previous studies assessing the performance of these formulations have mainly focused on broader spectral features in liquid systems and found that the formula $D(\omega) = \beta\hbar\omega(1 - \exp(-\beta\hbar\omega))^{-1}$ is most suitable.[37,38] However, as

we focus on a smaller spectral range of less than 1000 cm^{-1} we find that the various quantum correction factors have a very small effect on the general shape of the spectrum wherefore we will ignore this factor altogether and use $D(\omega) = 1$ (see also Fig. S3, ESI†).

3 Results and discussion

Initially, the geometries of the separated HCl and MeCN molecules and the MeCN–HCl cluster were optimized (Table S1, ESI†) and the vibrational modes were calculated within the harmonic oscillator approximation for reference (Table S2, ESI†). The MD simulation of the cluster was started from the optimized geometry. At suitable time intervals, the IR spectrum was created according to eqn (1) to check for convergence, using this as a metric for the quality of the statistical sampling. These spectra are shown in Fig. 1A, demonstrating a very slow convergence.

After 55 picoseconds of simulation (110,000 MD steps) the cluster decomposed and showed no sign of re-clustering, even after another 10,000 MD steps, wherefore the simulation was terminated (Fig. S4 and S5, ESI†). At this point, the main features of the spectrum had seemingly converged (black line in Fig. 1A), clearly showing a broad feature between 2400 and 2800 cm^{-1} and a smaller peak at *ca.* 2300 cm^{-1}. In the broad feature, several distinct peaks are visible including two shoulders around 2500 cm^{-1} and two peaks at *ca.* 2580 and 2625 cm^{-1}. The spectrum around the latter two peaks had not entirely converged when the cluster broke up, and given the large difference of the spectrum at the varying length of the MD run, it remains unclear whether this area would converge into one single feature.

Comparing this modelled spectrum with the experimental spectrum (Fig. S6, ESI†), some common features are seen such as the shape of the decay of the feature towards higher wavenumbers over a range *ca.* 200 cm^{-1}. However, the main feature between 2400 and 2800 cm^{-1} in the simulated spectrum is much wider than in the experimental spectrum. This discrepancy might be due to the chosen *ab initio* method or other computational parameters or due to insufficient phase-space sampling, but the precise reason remains unclear.

From the VDOS (Fig. 1B) it is seen that the peak at 2300 cm^{-1} originate from the stretch of the C–N triple bond, in accordance with the harmonic vibrational analysis, predicting a frequency of 2296 cm^{-1} (Table S2, ESI†). The major feature is clearly seen to originate from H–Cl vibration, with at most partial contribution from the N–C bond at the redshifted side of the feature. Nevertheless, the poor agreement of the modelled and experimental spectrum prevented us from gaining the desired information about the spectral shape of the H–Cl stretch band in the MeCH–HCl complex from this representation.

One of the major advantages of MD simulations over approaches based on structural optimizations is the much improved configurational sampling. We therefore initiated a thorough structural analysis of the configurations obtained from the MD simulation. Fig. 2 shows the correlation between the total potential energy and three selected geometrical parameters; the N–Cl distance and the N–H–Cl and C–N–H angles. The N–Cl distance is representative for the degree of dissociation of the cluster, whereas the N–H–Cl and C–N–H angles are representative for two most important cluster deformation modes. As expected, the potential energy is lowest at short N–Cl distances with a lesser dependence on the two angles.

In particular the C–N–H angle and to lesser extend the N–H–Cl angle, is clearly not most populated around the equilibrium configuration (in both cases 180.0°). The red histogram in Fig. 3 shows the population as a function of the N–H–Cl angle, while the corresponding graphs for the N–Cl distance and the C–N–H angle are shown in Fig. S7 and S8 (ESI†). For the N–H–Cl angle the most populated value is around 162°, while the linear configuration essentially is unpopulated (only 0.05% probability for the N–H–Cl angle exceeding 179.0°). This is in accordance with a microwave study of the HCN–HCl molecular complex by Legon *et al.*[39] concluding that "*the complex is linear at equilibrium but in the zero-point mode the subunits are undergoing fairly large amplitude excursions from this arrangement*," finding an average N–H–Cl

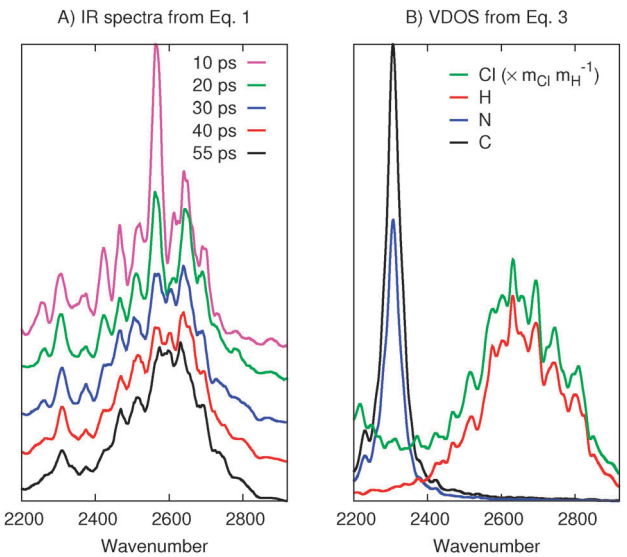

Fig. 1 (A) Modelled IR spectra of the MeCN–HCl complex at different lengths of the MD run (vertically shifted for clarity). (B) Velocity density of states in the 55 ps run (CH_3 atoms omitted).

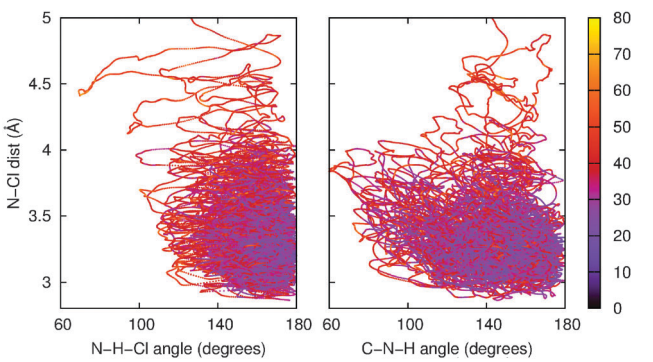

Fig. 2 Potential energy (in kJ mol^{-1}) as function of some descriptive structural parameters. After *ca.* 55 ps, the N–Cl distance exceeds 5 Å and the cluster decomposes.

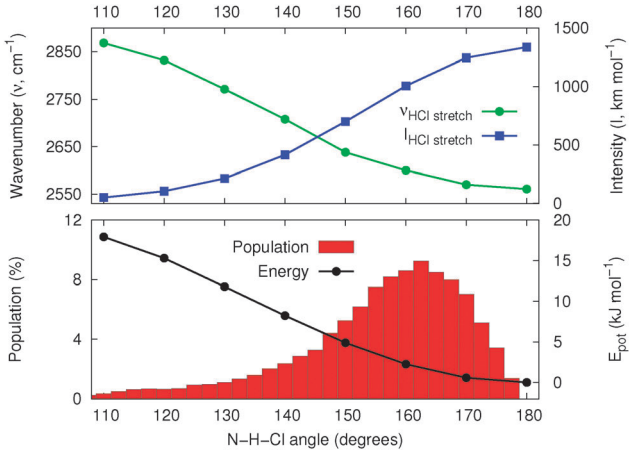

Fig. 3 A histogram of the population as function of the N–H–Cl angle. Harmonic H–Cl stretch wavenumbers (green), harmonic H–Cl stretch absorption intensities (blue), and potential energies (black) of optimized structures with fixed N–H–Cl angles. Structures are shown in Fig. 4.

angle of *ca.* 152°. This is an important property of clusters similar to these, fundamentally limiting the accuracy of the standard approach based on the linear global minimum energy structure at 0 K, motivating further analysis of this deformation mode.

Initially, a series of 22 configurations spaced by 2.5 pico seconds (*i.e.* 2.5 ps, 5.0 ps,..., 55 ps) were analysed for trends in the absorption intensities and wavenumbers depending on the N–H–Cl angle (Fig. S9 (ESI†) including also the N–Cl distance and the C–N–H angle). Although clear trends were found, these were not sufficiently strong for further analysis. Instead, this motivated a statistical based investigation where a series of structural optimizations were performed with the N–H–Cl angle constrained to given values between 110° and 180°. Unfortunately, constrained optimizations are currently not implemented in CP2K, so these calculations were performed using the Gaussian software package (Revision B.01).[40] We used the PBE functional with the aug-cc-pV(T+d)Z basis set[41,42] for minimum discrepancy between the MD data and the constrained optimizations. The resulting structures are shown in Fig. 4, and corresponding figures with constrained N–Cl distances and C–N–H angles are shown in Fig. S10 and S11 (ESI†), respectively.

On each constrained optimized geometry, the vibrational frequencies and absorption intensities were calculated using the harmonic oscillator approximation. These data are shown in Fig. 3, Fig. S7 and S8 (ESI†). The harmonic H–Cl frequencies are seen to vary from *ca.* 2200 to *ca.* 2900 cm^{-1} and the absorption intensities are seen to vary from less than 100 to more than 2600 km mol^{-1} in the populated range of geometries. Based on these data, the IR spectrum was re-modelled, using just a single degree of freedom as

$$A(\theta) \propto N(\theta) \times I(\theta) \quad (4)$$

where $N(\theta)$ denotes the population and $I(\theta)$ denotes the absorption intensity as functions of the geometrical parameter in question. This parameter is denoted θ, representing *e.g.* the N–H–Cl angle. For direct comparison with the experimental

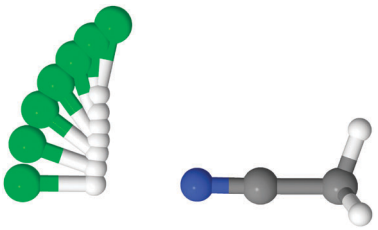

Fig. 4 Optimized geometries of the MeCN–HCl molecular complex at fixed N–H–Cl angles at the PBE/aug-cc-pV(T+d)Z level of theory. These geometries are used for calculating the wavenumbers, absorption intensities, and potential energy surface of the harmonic H–Cl stretch (see also Fig. 3).

spectrum, we obtained $A(\tilde{\nu})$ from $A(\theta)$ *via* the function $f(\theta) = \tilde{\nu}$. This function is shown as a green line if Fig. 3, also showing $N(\theta)$ and $I(\theta)$ as a red histogram and a blue line, respectively.

Fig. S12 and S13 (ESI†) show that the modelled spectra based on the N–Cl distance or the C–N–H angle differ significantly from the experimental spectrum. The former has significant absorbance in a 900 cm^{-1} broad feature, much broader than the experimental feature. The latter has significant absorbance in a feature ranging just *ca.* 30 cm^{-1}, much narrower than the experimental feature. We conclude that the constrained optimized structures shown in Fig. S10 and S11 (ESI†) do not represent the populated structures at 300 K well. However, the spectrum based on the N–H–Cl angle is seen to resemble both the shape and the width of the experimental spectrum and when shifted *ca.* 160 cm^{-1}, it matches the experimental spectrum very well (Fig. 5).

This observation confirms that the N–H–Cl bending mode is highly excited at 300 K as can already be deduced from the MD trajectory. Thus, we conclude that the experimental spectral anomaly, very likely, is a direct consequence of this deformation from the global minimum free energy structure. At present it is not clear to what extent this can be generalized to other hydrogen bonded systems, but it seems likely that this behaviour may be particularly pronounced in floppy systems where

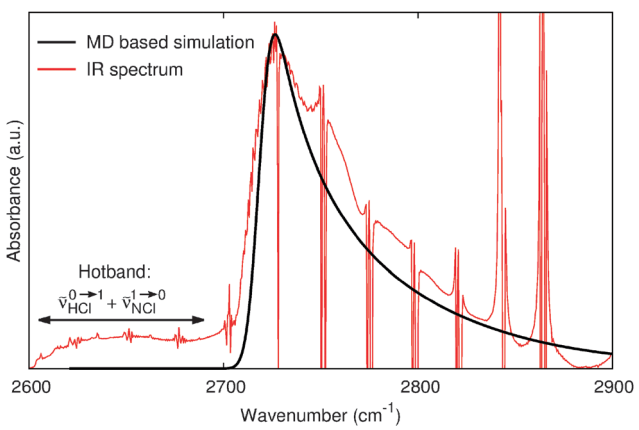

Fig. 5 Comparison of the experimental FTIR spectrum from Bork *et al.*[16] and the modelled spectrum using the N–H–Cl angle as the only variable degree of freedom. The modelled spectrum is blue-shifted 157 cm^{-1} and vertically scaled to maximize overlap. The sharp lines separated by 26 cm^{-1} are due to molecular HCl, not included in this study.

configurations other than the global minimum can be expected to have significant population.

Finally, we note that the feature between 2600 and 2700 cm^{-1} in the experimental spectrum has been attributed to the $\tilde{\nu}_{HCl}^{0\rightarrow1}$ + $\tilde{\nu}_{NCl}^{1\rightarrow0}$ hotband, which, as expected, is not reproduced by this simple analysis. The sharp lines in the experimental spectrum separated by *ca.* 26 cm^{-1} are due to molecular HCl that could not be fully subtracted from the recorded spectrum of the complex. As expected, these lines are not reproduced by the MD simulations either.

4 Conclusions

Motivated to solve the often found spectral anomalies of hydrogen bonded complexes, we have conducted an *ab initio* molecular dynamics study of the gas phase MeCN–HCl complex. The system was found to be very floppy and extended simulation time was required before convergence of the spectrum. Ultimately, the run was terminated by the irreversible decomposition of the cluster after 55 picoseconds (110,000 MD steps).

The resulting electric dipole moment data were autocorrelated and Fourier transformed to obtain the IR spectrum. Although several common features were seen, the agreement between the modelled spectrum and the experimental spectrum was not satisfactory. Likely causes include the chosen computational methods (PBE density functional, aug-TZV2P basis set, $(30\ Å)^3$ simulation box, 0.5 fs timestep, Nosé–Hoover thermostat) and insufficient configurational sampling.

The structural data from the MD run were used to investigate the most populated structures of the complex at 300 K. We mainly investigated the effects of three cluster deformation modes; the N–Cl distance and the C–N–H and the N–H–Cl angles. In three series of optimizations with either of these modes constrained, the H–Cl vibration frequencies and intensities were calculated. The spectrum was then re-modelled based on the H–Cl vibrational frequencies and absorption intensities from the constrained calculations, combined with the population data from the molecular dynamics simulations. For the N–H–Cl angle this yielded a spectrum in excellent agreement with the experimental spectrum, and we conclude that the spectral anomaly under investigation, very likely, is due to this cluster deformation mode.

One plausible explanation for the success of this approach *versus* the lack of success for the autocorrelation approach is the configurational sampling, providing a good enough description of each individual degree of freedom, most importantly the N–H–Cl angle, but an insufficient description of the coupling between modes, *e.g.* the coupling between the H–Cl and the N–H–Cl modes. The precise reason, however, remains unclear.

Finally, while investigating the populated values of the N–H–Cl angle we found that the global energy minimum structure (being linear) was essentially unpopulated and that the most populated value was 162°, in accordance with a microwave study on the HCN–HCl complex.[39] This clearly explains the discrepancy between any modelled spectrum based on the standard approach, *i.e.* frequency analysis of the linear, global minimum energy structure. Also, this demonstrates the advantages of investigating spectra based on molecular dynamics simulations.

Acknowledgements

We gratefully acknowledge the financial support by the Villum Foundation, the Maj and Tor Nessling Foundation (project #2011200), the Academy of Finland (Center of Excellence program, project #1118615, and LASTU program, project #135054), the Danish Council for Independent Research-Natural Science, and the European Research Council (project #257360 MOCA-PAF). We also thank the CSC-IT Center for Science Ltd and the Danish Centre for Scientific Computing for providing computational resources.

References

1 K. Müller-Dethlefs and P. Hobza, *Chem. Rev.*, 2000, **100**, 143–168.
2 M. W. Feyereisen, D. Feller and D. A. Dixon, *J. Phys. Chem.*, 1996, **100**, 2993–2997.
3 T. Kurtén, V. Loukonen, H. Vehkamäki and M. Kulmala, *Atmos. Chem. Phys.*, 2008, **8**, 4095–4103.
4 J. Almeida, S. Schobesberger, A. Kürten, I. K. Ortega, O. Kupiainen-Määttä, A. P. Praplan, A. Adamov, A. Amorim, F. Bianchi, M. Breitenlechner, A. David, J. Dommen, N. M. Donahue, A. Downard, E. Dunne, J. Duplissy, S. Ehrhart, R. C. Flagan, A. Franchin, R. Guida, J. Hakala, A. Hansel, M. Heinritzi, H. Henschel, T. Jokinen, H. Junninen, M. Kajos, J. Kangasluoma, H. Keskinen, A. Kupc, T. Kurtén, A. N. Kvashin, A. Laaksonen, K. Lehtipalo, M. Leiminger, J. Leppä, V. Loukonen, V. Makhmutov, S. Mathot, M. J. McGrath, T. Nieminen, T. Olenius, A. Onnela, T. Petäjä, F. Riccobono, I. Riipinen, M. Rissanen, L. Rondo, T. Ruuskanen, F. D. Santos, N. Sarnela, S. Schallhart, R. Schnitzhofer, J. H. Seinfeld, M. Simon, M. Sipilä, Y. Stozhkov, F. Stratmann, A. Tomé, J. Tröstl, G. Tsagkogeorgas, P. Vaattovaara, Y. Viisanen, A. Virtanen, A. Vrtala, P. E. Wagner, E. Weingartner, H. Wex, C. Williamson, D. Wimmer, P. Ye, T. Yli-Juuti, K. S. Carslaw, M. Kulmala, J. Curtius, U. Baltensperger, D. R. Worsnop, H. Vehkamäki and J. Kirkby, *Nature*, 2013, **502**, 359–363.
5 J. Kirkby, J. Curtius, J. Almeida, E. Dunne, J. Duplissy, S. Ehrhart, A. Franchin, S. Gagne, L. Ickes, A. Kurten, A. Kupc, A. Metzger, F. Riccobono, L. Rondo, S. Schobesberger, G. Tsagkogeorgas, D. Wimmer, A. Amorim, F. Bianchi, M. Breitenlechner, A. David, J. Dommen, A. Downard, M. Ehn, R. C. Flagan, S. Haider, A. Hansel, D. Hauser, W. Jud, H. Junninen, F. Kreissl, A. Kvashin, A. Laaksonen, K. Lehtipalo, J. Lima, E. R. Lovejoy, V. Makhmutov, S. Mathot, J. Mikkila, P. Minginette, S. Mogo, T. Nieminen, A. Onnela, P. Pereira, T. Petaja, R. Schnitzhofer, J. H. Seinfeld, M. Sipila, Y. Stozhkov, F. Stratmann, A. Tome, J. Vanhanen, Y. Viisanen, A. Vrtala, P. E. Wagner, H. Walther, E. Weingartner, H. Wex, P. M. Winkler, K. S. Carslaw, D. R. Worsnop, U. Baltensperger and M. Kulmala, *Nature*, 2011, **476**, 429–435.

6 X. Ge, A. S. Wexler and S. L. Clegg, *Atmos. Environ.*, 2011, **45**, 524–546.
7 S. Chung and M. Hippler, *J. Chem. Phys.*, 2006, **124**, 214316.
8 M. Hippler, *J. Chem. Phys.*, 2007, **127**, 084306.
9 M. Hippler, S. Hesse and M. A. Suhm, *Phys. Chem. Chem. Phys.*, 2010, **12**, 13555–13565.
10 D. L. Howard and H. G. Kjaergaard, *J. Phys. Chem. A*, 2006, **110**, 9597–9601.
11 D. L. Howard and H. G. Kjaergaard, *Phys. Chem. Chem. Phys.*, 2008, **10**, 4113–4118.
12 L. Du and H. G. Kjaergaard, *J. Phys. Chem. A*, 2011, **115**, 12097–12104.
13 L. Du, K. Mackeprang and H. G. Kjaergaard, *Phys. Chem. Chem. Phys.*, 2013, **15**, 10194–10206.
14 L. Du, J. R. Lane and H. G. Kjaergaard, *J. Chem. Phys.*, 2012, **136**, 184305.
15 N. Bork, L. Du and H. G. Kjaergaard, *J. Phys. Chem. A*, 2014, **118**, 1384–1389.
16 N. Bork, L. Du, H. Reiman, T. Kurtén and H. G. Kjaergaard, *J. Phys. Chem. A*, 2014, **118**, 5316–5322.
17 A. L. Garden, L. Halonen and H. G. Kjaergaard, *J. Phys. Chem. A*, 2008, **112**, 7439–7447.
18 D. Bégué, I. Baraille, P. Garrain, A. Dargelos and T. Tassaing, *J. Chem. Phys.*, 2010, **133**, 034102.
19 M.-P. Gaigeot, M. Martinez and R. Vuilleumier, *Mol. Phys.*, 2007, **105**, 2857–2878.
20 K. Mackeprang, H. G. Kjaergaard, T. Salmi, V. Hänninen and L. Halonen, *J. Chem. Phys.*, 2014, **140**, 184309.
21 V. Loukonen, I-F. W. Kuo, M. J. McGrath and H. Vehkamäki, *Chem. Phys.*, 2014, **428**, 164–174.
22 D. Marx and J. Hutter, *Ab initio molecular dynamics: basic theory and advanced methods*, Cambridge University Press, 2009.
23 D. McQuarrie, *Statistical mechanics*, University Science, Sausalito, USA, 2000.
24 G. Lippert, J. Hutter and M. Parrinello, *Theor. Chem. Acc.*, 1999, **103**, 124–140.
25 B. Lippert, J. Hutter and M. Parrinello, *Mol. Phys.*, 1997, **92**, 477–488.
26 J. VandeVondele, M. Krack, F. Mohamed, M. Parrinello, T. Chassaing and J. Hutter, *Comput. Phys. Commun.*, 2005, **167**, 103–128.
27 J. VandeVondele and J. Hutter, *J. Chem. Phys.*, 2007, **127**, 114105.
28 V. Loukonen, N. Bork and H. Vehkamäki, *Mol. Phys.*, 2014, **112**, 1979–1986.
29 N. Bork, V. Loukonen and H. Vehkamaki, *J. Phys. Chem. A*, 2013, **117**, 3143–3148.
30 J. Perdew, K. Burke and M. Ernzerhof, *Phys. Rev. Lett.*, 1996, **77**, 3865–3868.
31 J. Elm, M. Bilde and K. V. Mikkelsen, *J. Chem. Theory Comput.*, 2012, **8**, 2071–2077.
32 H. R. Leverentz, J. I. Siepmann, D. G. Truhlar, V. Loukonen and H. Vehkamaki, *J. Phys. Chem. A*, 2013, **117**, 3819–3825.
33 S. Grimme, J. Antony, S. Ehrlich and H. Krieg, *J. Chem. Phys.*, 2010, **132**, 154104.
34 N. Bork, N. Bonanos, J. Rossmeisl and T. Vegge, *Phys. Chem. Chem. Phys.*, 2011, **13**, 15256–15263.
35 G. J. Martyna, M. L. Klein and M. Tuckerman, *J. Chem. Phys.*, 1992, **97**, 2635–2643.
36 N. Marzari, A. A. Mostofi, J. R. Yates, I. Souza and D. Vanderbilt, *Rev. Mod. Phys.*, 2012, **84**, 1419–1475.
37 H. Ahlborn, B. Space and P. B. Moore, *J. Chem. Phys.*, 2000, **112**, 8083–8088.
38 M.-P. Gaigeot and M. Sprik, *J. Phys. Chem. B*, 2003, **107**, 10344–10358.
39 A. Legon, E. Campbell and W. Flygare, *J. Chem. Phys.*, 1982, **76**, 2267.
40 M. J. Frisch, G. W. Trucks, H. B. Schlegel, G. E. Scuseria, M. A. Robb, J. R. Cheeseman, G. Scalmani, V. Barone, B. Mennucci, G. A. Petersson, H. Nakatsuji, M. Caricato, X. Li, H. P. Hratchian, A. F. Izmaylov, J. Bloino, G. Zheng, J. L. Sonnenberg, M. Hada, M. Ehara, K. Toyota, R. Fukuda, J. Hasegawa, M. Ishida, T. Nakajima, Y. Honda, O. Kitao, H. Nakai, T. Vreven, J. A. Montgomery, Jr., J. E. Peralta, F. Ogliaro, M. Bearpark, J. J. Heyd, E. Brothers, K. N. Kudin, V. N. Staroverov, R. Kobayashi, J. Normand, K. Raghavachari, A. Rendell, J. C. Burant, S. S. Iyengar, J. Tomasi, M. Cossi, N. Rega, J. M. Millam, M. Klene, J. E. Knox, J. B. Cross, V. Bakken, C. Adamo, J. Jaramillo, R. Gomperts, R. E. Stratmann, O. Yazyev, A. J. Austin, R. Cammi, C. Pomelli, J. W. Ochterski, R. L. Martin, K. Morokuma, V. G. Zakrzewski, G. A. Voth, P. Salvador, J. J. Dannenberg, S. Dapprich, A. D. Daniels, Ö. Farkas, J. B. Foresman, J. V. Ortiz, J. Cioslowski and D. J. Fox, *Gaussian09 Revision B.01*, Gaussian Inc, Wallingford CT, 2009.
41 T. H. J. Dunning, *J. Chem. Phys.*, 1989, **90**, 1007–1023.
42 T. Dunning Jr, K. Peterson and A. Wilson, *J. Chem. Phys.*, 2001, **114**, 9244.

